Applied Probability Trust (27 June 2011)

TOPOLOGICAL RELATIONSHIPS IN SPATIAL TESSELLATIONS.

VIOLA WEISS,* *Fachhochschule Jena*

RICHARD COWAN,** *University of Sydney*

Abstract

Tessellations of $\mathbb{R}^3$ that use convex polyhedral cells to fill the space can be extremely complicated. This is especially so for tessellations which are not 'facet-to-facet', that is, for those where the facets of a cell do not necessarily coincide with the facets of that cell's neighbours. Adjacency concepts between neighbouring cells (or between neighbouring cell elements) are not easily formulated when facets do not coincide. In this paper, we make the first systematic study of these topological relationships when a tessellation of $\mathbb{R}^3$ is not facet-to-facet. The results derived can also be applied to the simpler facet-to-facet case. Our study deals with both random tessellations and deterministic 'tilings'. Some new theory for planar tessellations is also given.

Keywords: random geometry, tessellations, tilings, packing of polyhedra, space-filling, topology.

2000 Mathematics Subject Classification: Primary 60D05; 05B45; 52C17
Secondary 60G55; 51M20; 52B10

1. Introduction

In this paper we study *random stationary spatial tessellations*, that is, random tessellations of the three-dimensional space $\mathbb{R}^3$ having statistical properties that are invariant under translation. We develop new mean-value formulae for various topological parameters in cases where the cells of the tessellation are convex polyhedra. The formulae generalize one of the identities for stationary planar tessellations presented by the second author ([2], [3]) in 1978. These identities, using notations based on his later papers ([4], [7]), are:

$$\mu = \frac{2\theta}{\theta - 2} \tag{1}$$

$$\nu = \frac{2(\theta - \phi)}{\theta - 2}. \tag{2}$$

* Postal address: Fachhochschule Jena, D-07703 Jena, Germany. Viola.Weiss@fh-jena.de
** Postal address: School of Mathematics and Statistics, University of Sydney, NSW, 2006, Australia. rcowan@usyd.edu.au

Here μ indicates, for a typical cell, the expected number of *edges* (or *vertices*) of the tessellation on the cell's boundary. The entity ν is the expected number of *sides* (or *corners*) that the typical cell has. For a typical tessellation vertex, θ is the mean number of emanating edges. If a vertex has j emanating edges, there are j angles subtended by these edges at the vertex; if one of these angles is equal to π, the vertex is called a π*-vertex*. The parameter ϕ is defined as the proportion of vertices which are π-vertices. The words 'vertex' and 'edge' refer to the tessellation, whilst 'corner' and 'side' are words used for the 0-faces and 1-faces of the convex polygonal cells.

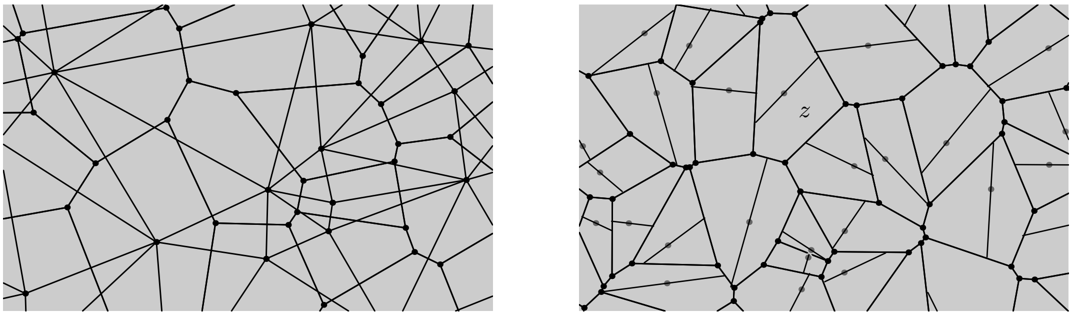

(a) (b)

FIGURE 1: (a) The planar tessellation formed as the superposition of a Poisson-Voronoi tessellation and its Poisson-Delaunay 'dual'. The tessellation is *side-to-side* – every edge is a 'side' of the two polygonal cells that it separates. Side-to-side tessellations have no π-vertices. (b) A Voronoi tessellation with each cell split by a random chord through the point used to generate that cell. These generating points are shown in grey; they are not tessellation vertices. Note that half of all vertices of the tessellation are π-vertices. The cell marked "z" has five sides and seven edges on its boundary.

The two entities μ and ν are equal for a *side-to-side* tessellation (see Figure 1(a) for a definition of this terminology and an example), but differ if there exist π-vertices as in the example of Figure 1(b).

We illustrate formulae (1) and (2) with four examples. In Figure 1(a), suppose that the Poisson point process that generates the tessellation has intensity ρ. Then the vertex-intensities of the Delaunay and Voronoi components of the tessellation are ρ and 2ρ respectively. It is known (Muche [21]) that the intensity of the edge-crossings of these two components is 4ρ. So $\theta = (6 \times \rho + 3 \times 2\rho + 4 \times 4\rho)/7\rho = 4$. Since $\phi = 0$, we can write $\mu = \nu = 4$.

In Figure 1(b), both the Voronoi vertices and the new vertices created by the random chords have intensity 2ρ. So $\phi = \frac{1}{2}$. Each type is always of order three, so $\theta = 3$. Therefore $\mu = 6$ and $\nu = 5$.

The other two examples are based on Figure 2. In Figure 2(a), a realisation of the so-called STIT model of Nagel and Weiss ([22], [14]) is shown. Here the tessellation within the window is constructed by successive division of cells (in a particular manner) by independent random chords. This is one of a wide class of tessellations (recently systemised in Cowan [6]) which can be constructed in an iterative way. Many such constructions have similar characteristics to this picture, with all vertices being π-vertices and having order 3. Thus $\phi = 1$ and $\theta = 3$; so $\mu = 6$ and $\nu = 4$. Although not constructed by iterative division of cells, we note that one of the Arak class of models ([1], [17]) has similar parameters and so a similar calculation.

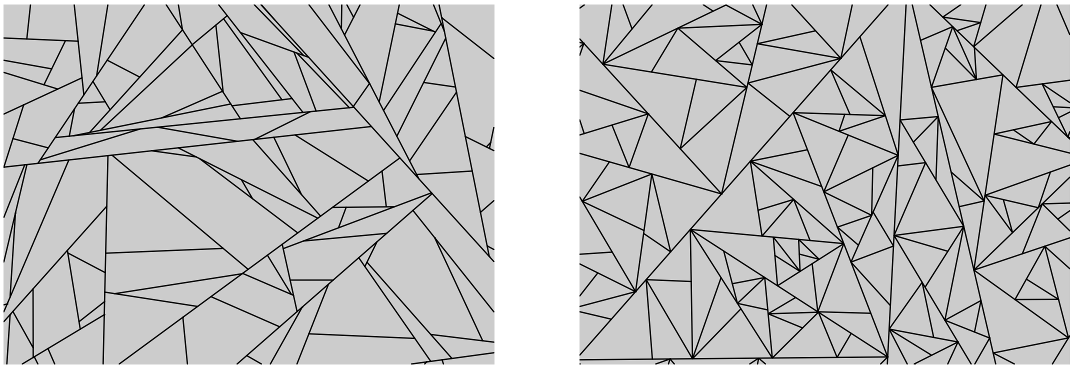

(a) (b)

FIGURE 2: (a) A realisation of the STIT model within a rectangular viewing window. (b) This tessellation is constructed by successive division of cells with independent random chords, commencing with a bounded triangular window which is the first cell in the process (the *ancestor*). The division chord is drawn from a randomly-selected corner of the triangle to a random point on the opposite side, thereby creating two triangular *daughter* cells. This rule is applied iteratively, with dilation to keep the line-intensity and mean cell size constant, to yield a tessellation comprising only triangular cells. If this construction converges to a stationary locally-finite tessellation of $\mathbb{R}^2$ (an issue still under consideration in our studies), its realisation will look like the figure.

The tessellation in Figure 2(b) also comes from the iterative division of cells, but it starts with a triangular window and all random chords are constrained to create only triangular cells (see caption and Cowan ([5], [6])). Here, too, all vertices are π-vertices and all cells have three sides (so $\phi = 1$ and $\nu = 3$). Therefore from (2),

$$3 = \frac{2(\theta - 1)}{\theta - 2},$$

which implies that $\theta = 4$. From (1), $\mu = 4$.

These examples illustrate that (2) is an essential adjunct to (1). In all the examples, we note that the fundamental parameters θ and ϕ satisfy the general constraints:

$$0 \leq \phi \leq 1; \qquad\qquad 3 \leq \theta \leq 6 - 2\phi. \tag{3}$$

These constraints, which improve those derived by Kendall and Mecke [9] who made no use of ϕ, apply to (1) and (2). The upper bound on θ, which has not been reported before, follows from (2) and $\nu \geq 3$.

Strangely, few authors have paid any attention to the difference between *edges* and *sides*. Mecke [11] develops (1), but not (2), and the standard text of Stoyan, Kendall and Mecke ([28], Sections 10.3 and 10.4) includes only (1) in a list of identities for stationary planar tessellations. In $\mathbb{R}^3$, there has been no discussion of the analogues of (2), although there have been generalisations of (1) (see Radecke [25], Mecke [12] and Stoyan et al [28], together with the d-dimensional study of Møller [18].) Likewise in the influential book of Schneider and Weil ([26], Chapter 10) which discusses tessellations of $\mathbb{R}^d, d \geq 2$, only the facet-to-facet case is treated (though they use the equivalent concept, *face-to-face*). These books and papers do not discuss the rather complicated issues that arise in three-dimensional tessellations which are not *facet-to-facet*.

Formula (2) is shown to be valid, for the planar case with non-convex cells and curved edges, in Cowan and Tsang [7] — but the issue is not discussed in the studies of planar structures with curved cell-boundaries by either Stoyan [27] or Miles [16]. Nor has there been reference to formulae like (2) in the studies of more general tessellations, those where the structure is a cell-complex in $\mathbb{R}^d$ constructed with various systems of non-convex cells (Weiss and Zähle [30], Zähle [31], Leistritz and Zähle [10]). This is perhaps understandable as those cell-complex papers deal with purely topological structures not tainted by the geometric concepts of 'angles equal to π'.

So there is a gap in the literature; our current paper fills this gap. It provides the first systematic study of the complications in $\mathbb{R}^3$ when a tessellation is not *facet-to-facet*, whilst also giving some new theory for the planar case.

2. Notational style

With some exceptions that we have cited, the studies mentioned above deal only with the *primitive elements* of the tessellation: in the planar case, the *vertices*, *edges* and *cells* of the planar graph that the structure creates. In $\mathbb{R}^3$, the two-dimensional polygonal *plates* which separate the three-dimensional cells are also considered, along with *vertices*, *edges* and *cells*. All of these entities are convex polytopes.

These primitive elements are sometimes referred to as 0-cells, 1-cells, 2-cells and (in the spatial case) 3-cells, reflecting the dimension of the element – in keeping with cell-complex theory. This has led to notations such as μ_{ij} := the expected number of j-cells adjacent to the typical i-cell and λ_i := the intensity of i-cells – by which is meant the intensity of the point-process of centroids of i-cells. For example, μ_{01} is the expected number of edges 'adjacent to' (that is, 'emanating from') the typical vertex – Cowan's θ in the planar case.

We note that for each class of objects in the realised tessellation there is a point process formed from the objects' centroids. When the class comprises a primitive type of element, the point process is simple – that is, all centroids are distinct points of the Euclidean space, so there are no 'multiple points' of the point process. Later, when we consider other objects, the centroids will often coincide, forming a non-simple point process with multiplicities. For example in $\mathbb{R}^2$, the corners of cells will induce a point process with a multiplicity at each vertex of the tessellation – and the centroid of a cell's side will often coincide with the centroid of a neighbouring cell's side, giving a multiplicity of 2. Indeed the two sides in such cases will often coincide – they are the same geometric object, distinguished by the implicit link each has to a cell.

Because our study looks at many objects which have the same dimension, we are unable to rely solely on subscripts which convey the object's dimension. For example, in $\mathbb{R}^2$ the symbol μ_{21} would be ambiguous, meaning both the *expected number of edges* and the *expected number of sides* adjacent to a typical cell – because *edges* and *sides* are both of dimension one.

Instead we use letter subscripts for the primitive elements, namely V, E, P and Z for the following object-classes – *vertices*, *edges*, *plates* and *cells* ('Z for Zellen', used instead of 'C for cell' because one of us has used 'C for corner' in earlier work).

For objects which are the faces of primitives, for example the sides (1-faces) and corners (0-faces) of *polygonal* primitives (such as cells in $\mathbb{R}^2$ or plates in $\mathbb{R}^3$), we retain some use of dimensional subscripts whilst conveying by letter the type of primitive element which 'owns' the face.

Definition 1. *Let X be a class of convex polytopes, each member of the class having dimension $i \le 3$. Define $X_j,\ j < i$, as the class of objects which are j-dimensional faces (j-faces) of some polytope $\in X$. Further nesting is allowed, so $(X_j)_k,\ k < j < i$, denotes the class of objects which are k-faces of a j-face of some object $\in X$. An object $\in X$ is often referred to as "an X-type object" or "an object of type X".*

In $\mathbb{R}^2$ for example, an object of type Z_1 is a side of a cell, Z_0 denotes the objects which are corners of cells and E_0 is the class of termini of edges. In $\mathbb{R}^3$, objects of types P_1 and $(Z_2)_1$ are respectively a side of a plate and a side of a facet (which is a 2-face of a cell). A 0-face or 1-face of a three-dimensional polyhedral cell – called an *apex* or *ridge* respectively – is in the class Z_0 or Z_1. A terminus of a ridge is type $(Z_1)_0$. Because of possibly multiplicities, discussed above, some of these classes are multi-sets.

Remark 1. *For some purposes, it may be necessary to emphasise the ownership of an object in X_j. For example, when considering a cell-corner $z_0 \in Z_0$, we might wish to distinguish this corner from the other cell-corners at the same position. In that circumstance, we must place an ownership 'mark' on each element of Z_0, and deal with a product space $Z_0^+ := Z_0 \times M$, where M is the mark space comprising elements of Z. In this paper, we have no need for this augmentation; Definition 1 is sufficient.*

The notation in Definition 1 appears complicated, but many simpler styles were tried and found inadequate. We shall assist verbally where appropriate, however, referring to an object's face as *facet*, *ridge* or *apex* for objects which are polyhedra, *side* or *corner* for polygons and *terminus* for line-segments.

Subsets of the class X are denoted by $X[\cdot]$, with the contents of the $[\cdot]$ being a suitably suggestive symbol introduced in an *ad hoc* manner. For example in $\mathbb{R}^2$, the sub-class of π-vertices is $V[\pi]$.

We now formalize the notation for 'object intensity' and concept of 'adjacent objects'.

Definition 2. *The intensity of objects belonging to class X is denoted by λ_X.*

Definition 3. *An object $x \in X$ is said to be* adjacent to *an object $y \in Y$ if either $x \subseteq y$ or $y \subseteq x$. For any $x \in X$, the number of objects of type Y adjacent to x is denoted by $m_Y(x)$. For a random tessellation we define μ_{XY} as the expected value of $m_Y(x)$ when x is the typical member of X. Formally, we write $\mu_{XY} := \mathsf{E}_X(m_Y(x)) = \int m_Y(x)\mathsf{P}_X(dx)$, where E_X denotes an expectation for the typical object of type X (that is, defined with respect to the Palm measure P_X, see [28]). Also $\mu_{XY}^{(2)} := \mathsf{E}_X(m_Y(x)^2)$.*

If $B(r)$ is the ball of radius r centred at the origin, μ_{XY} can also be defined formally as

$$\mu_{XY} := \lim_{r\to\infty} \frac{\sum_{\{x\in X:\ \text{centroid of } x \text{ is } \in B(r)\}} m_Y(x)}{\text{number of objects of type } X \text{ with centroid } \in B(r)}, \tag{4}$$

when the limit shown is a constant. This is so for ergodic tessellations ([2], [3]) and for regular *tilings* with an infinitely-repeated sub-unit of cells (as in [8]). This latter type can be made to fit our *random stationary* framework by locating the origin O uniformly distributed within one copy of the repeating sub-unit. The limit in (4) is also a constant for many tessellations that have a 'tiling component', for example, those randomly constructed from a tiling or those mixed with or superimposed on a tiling.

When X and Y are both primitive-element classes, it has been shown in [11], [30] and [10] that

$$\lambda_X \mu_{XY} = \lambda_Y \mu_{YX} \tag{5}$$

and this identity also holds when either X or Y or both are classes of *faces of primitives*; Møller's Theorem 5.1 [18] provides the proof of this extension. For example, when discussing *sides of plates*, $\lambda_{P_1}\mu_{P_1 Z} = \lambda_Z \mu_{Z P_1}$.

We can express θ and ϕ, symbols used by Cowan in planar tessellations, by using the adjacency notation; $\theta = \mu_{VE}$ and $\phi = \mu_{V\mathring{Z}_1}$, the expected number of 'side-interiors' adjacent to a typical vertex (where the *interior* of a side, or indeed of any object x of lower dimension than the space of the tessellation, is defined using the *relative topology* on x). Also $\mathring{X}$ denotes the class comprising the *relative interiors* of objects in class X (and ∂X denotes the class comprising *boundaries*, defined once more using the appropriate relative topology). Whilst we drop the usage of θ from this point, preferring μ_{VE}, we retain ϕ.

3. Known results for the primitive elements

For the primitive objects in a planar tessellation, the following table gives the known values of λ_X and μ_{XY}. The table, based on the studies cited above, includes formula (1).

X	λ_X/λ_V
vertices V	1
edges E	$\frac{1}{2}\mu_{VE}$
cells Z	$\frac{\mu_{VE}-2}{2}$

(a)

μ	V	E	Z
V	1	μ_{VE}	μ_{VE}
E	2	1	2
Z	$\frac{2\mu_{VE}}{\mu_{VE}-2}$	$\frac{2\mu_{VE}}{\mu_{VE}-2}$	1

(b)

Table 1: Results for the primitive elements in tessellations of $\mathbb{R}^2$. (a) λ_X values for $X \in \{V, E, Z\}$. Note that $\lambda_V - \lambda_E + \lambda_Z = 0$. (b) μ_{XY} when both X and Y are $\in \{V, E, Z\}$. Note the validity of (5). We also note that $\lambda_{V[\pi]} = \phi\lambda_V$.

Also known are the same entities for the primitive elements of spatial tessellations. In Table 2, we write these in terms of μ_{VE}, μ_{EP} and μ_{PV}, a trio with cyclic subscripts, and use

$$f(x) := \mu_{VE}\ \mu_{EP} - x\ (\mu_{VE} - 2) \tag{6}$$

as a useful abbreviation.

X	λ_X/λ_V
vertices V	1
edges E	$\frac{1}{2}\mu_{VE}$
plates P	$\dfrac{\mu_{VE}\,\mu_{EP}}{2\mu_{PV}}$
cells Z	$\dfrac{f(\mu_{PV})}{2\mu_{PV}}$

(a)

μ	V	E	P	Z
V	1	μ_{VE}	$\frac{1}{2}\mu_{VE}\,\mu_{EP}$	$\frac{1}{2}f(2)$
E	2	1	μ_{EP}	μ_{EP}
P	μ_{PV}	μ_{PV}	1	2
Z	$\dfrac{\mu_{PV}f(2)}{f(\mu_{PV})}$	$\dfrac{\mu_{VE}\,\mu_{EP}\,\mu_{PV}}{f(\mu_{PV})}$	$\dfrac{2\mu_{VE}\,\mu_{EP}}{f(\mu_{PV})}$	1

(b)

Table 2: Results in $\mathbb{R}^3$ using the abbreviation f, defined by (6). (a) λ_X when $X \in \{V, E, P, Z\}$. Note that $\lambda_V - \lambda_E + \lambda_P - \lambda_Z = 0$. (b) Values of μ_{XY} for primitive-element classes X and Y. Note that $\mu_{VE} - \mu_{VP} + \mu_{VZ} = 2$ and $\mu_{ZV} - \mu_{ZE} + \mu_{ZP} = 2$.

4. The faces of primitive elements: planar case

We now calculate some results for *faces of the primitive elements*, dealing with the planar case first. To find λ_{Z_1}, the intensity of sides, we note that $\mu_{Z_1E} - \mu_{\overset{\circ}{Z_1}V} = 1$. Therefore

$$\begin{aligned}\lambda_{Z_1} &= \lambda_{Z_1}\mu_{Z_1E} - \lambda_{Z_1}\mu_{\overset{\circ}{Z_1}V} \\ &= \lambda_E\mu_{EZ_1} - \lambda_V\mu_{V\overset{\circ}{Z_1}} \\ &= 2\lambda_E - \phi\lambda_V \\ &= (\mu_{VE} - \phi)\lambda_V, \end{aligned} \tag{7}$$

using identity (5), $\phi = \mu_{V\overset{\circ}{Z_1}}$ (each vertex being adjacent to either 0 or 1 side-interiors) and the obvious $\mu_{EZ_1} = 2$ (each edge being adjacent to two sides).

Formulae (7) leads on to formula (2) – with assistance from some new notation which generalizes Cowan's entity ν.

Definition 4. *Let X be a class of convex polytopes, all members of which have dimension i. For $j < i$, we define $n_j(x)$ as the number of j-faces of a particular object $x \in X$. Define $\nu_j(X) := \mathsf{E}_X(n_j(x))$, the expected number for the typical X-object.*

The notation allows nesting; for example $\nu_k(X_j)$ is the expected number of k-faces of the typical object of type X_j ($k < j < i$, where $i = \dim x,\ \forall x \in X$). An example with two levels of nesting occurs in spatial tessellations: $\nu_0((Z_2)_1)$ is the expected number of termini of a typical 'side of a facet' of a cell.

Some examples of the definition in the fairly simple planar case are as follows.

- $\nu_1(Z)$ = Cowan's ν, the expected number of sides of the typical cell. We can write $\lambda_{Z_1} = \lambda_Z\ \nu_1(Z)$. Therefore, using (7) and Table 1,

$$\nu_1(Z) = \frac{\lambda_{Z_1}}{\lambda_Z} = \frac{2(\mu_{VE} - \phi)}{\mu_{VE} - 2}, \tag{8}$$

providing a fresh proof of Cowan's (2). Of course, $\nu_0(Z) = \nu_1(Z)$ and this leads to $\lambda_{Z_0} = \lambda_Z\ \nu_0(Z) = (\mu_{VE} - \phi)\ \lambda_V$.

- $\nu_0(E)$ = the mean number of edge-termini of the typical edge. Trivially $\nu_0(E) = 2$, so $\lambda_{E_0} = \lambda_E\ \nu_0(E) = \mu_{VE}\ \lambda_V$.
- $\nu_0(Z_1)$ = the mean number of side-termini of the typical side. Obviously $\nu_0(Z_1) = 2$, so $\lambda_{(Z_1)_0} = \lambda_{Z_1}\ \nu_0(Z_1) = 2(\mu_{VE} - \phi)\lambda_V$.

Table 3 summarizes the planar λ- and ν-results expressed in terms of μ_{VE} and ϕ.

X	λ_X/λ_V
termini E_0	μ_{VE}
corners Z_0	$\mu_{VE} - \phi$
sides Z_1	$\mu_{VE} - \phi$
side-termini $(Z_1)_0$	$2(\mu_{VE} - \phi)$

(a)

X	$\nu_0(X)$	$\nu_1(X)$
edges E	2	-
sides Z_1	2	-
cells Z	$\dfrac{2(\mu_{VE} - \phi)}{\mu_{VE} - 2}$	$\dfrac{2(\mu_{VE} - \phi)}{\mu_{VE} - 2}$

(b)

Table 3: Results for faces of the primitive elements (and faces of faces) in planar tessellations. (a) λ_X values for $X \in \{E_0, Z_0, Z_1, (Z_1)_0\}$. (b) Values of $\nu_j(X),\ j \leq 1$ for $X \in \{E, Z_1, Z\}$.

Table 4 gives various planar μ-results, proved in Appendix A. Many of these results use the second moment, $\mu_{VE}^{(2)}$, and $\mu_{V[\pi]E}$, the expected number of edges adjacent to the typical π-vertex. The following function is a useful abbreviation:

$$
\begin{aligned}
g(x) &:= \mu_{VE}^{(2)} - x\ \phi\ \mu_{V[\pi]E}, & \phi > 0 \\
&= \mu_{VE}^{(2)} & \phi = 0.
\end{aligned}
\tag{9}
$$

μ	V	E	Z
E_0	1	$\dfrac{\mu_{VE}^{(2)}}{\mu_{VE}}$	$\dfrac{\mu_{VE}^{(2)}}{\mu_{VE}}$
$(Z_1)_0$	1	$\dfrac{g(1)}{\mu_{VE} - \phi}$	$\dfrac{g(1)}{\mu_{VE} - \phi}$
Z_0	1	$\dfrac{g(1)}{\mu_{VE} - \phi}$	$\dfrac{g(1)}{\mu_{VE} - \phi}$
Z_1	$\dfrac{2\mu_{VE} - \phi}{\mu_{VE} - \phi}$	$\dfrac{\mu_{VE}}{\mu_{VE} - \phi}$	-

μ	E_0	$(Z_1)_0$	Z_0	Z_1
V	μ_{VE}	$2(\mu_{VE} - \phi)$	$\mu_{VE} - \phi$	$2\ \mu_{VE} - \phi$
E	$\dfrac{2\ \mu_{VE}^{(2)}}{\mu_{VE}}$	$\dfrac{4\ g(1)}{\mu_{VE}}$	$\dfrac{2\ g(1)}{\mu_{VE}}$	2
Z	$\dfrac{2\ \mu_{VE}^{(2)}}{\mu_{VE} - 2}$	$\dfrac{4\ g(1)}{\mu_{VE} - 2}$	$\dfrac{2\ g(1)}{\mu_{VE} - 2}$	-
E_0	$\dfrac{\mu_{VE}^{(2)}}{\mu_{VE}}$	$\dfrac{2\ g(1)}{\mu_{VE}}$	$\dfrac{g(1)}{\mu_{VE}}$	$\dfrac{2\ g(\frac{1}{2})}{\mu_{VE}}$
$(Z_1)_0$	$\dfrac{g(1)}{\mu_{VE} - \phi}$	$\dfrac{2(g(2) + \phi)}{\mu_{VE} - \phi}$	$\dfrac{g(2) + \phi}{\mu_{VE} - \phi}$	$\dfrac{2\ g(\frac{3}{2}) + \phi}{\mu_{VE} - \phi}$
Z_0	$\dfrac{g(1)}{\mu_{VE} - \phi}$	$\dfrac{2(g(2) + \phi)}{\mu_{VE} - \phi}$	$\dfrac{g(2) + \phi}{\mu_{VE} - \phi}$	$\dfrac{2\ g(\frac{3}{2}) + \phi}{\mu_{VE} - \phi}$
Z_1	$\dfrac{2\ g(\frac{1}{2})}{\mu_{VE} - \phi}$	$\dfrac{2(2\ g(\frac{3}{2}) + \phi)}{\mu_{VE} - \phi}$	$\dfrac{2\ g(\frac{3}{2}) + \phi}{\mu_{VE} - \phi}$	-

Table 4: Further μ_{XY} values for the primitive-element classes V, E and Z in a planar tessellation, and for those classes, $E_0, (Z_1)_0, Z_0$ and Z_1, whose members are faces of (or faces of faces of) primitives. These supplement those μ_{XY} values in Table 2(b). The function g is defined in (9).

We conclude our material on planar tessellations by restating that our results summarised in Tables 1, 3 and 4 should be read with the constraints of (3) in mind.

5. Description of facets in a spatial tessellation

The situation in $\mathbb{R}^3$ has much greater complexity, as seen in Figure 3 which shows a particular facet z_2 of a cell – plus some of the other cells that 'interact' with it. In (a), we note that z_2 comprises 8 polygonal plates. The interior of z_2 has considerable structure; it contains three vertices and 10 edge-interiors of the tessellation. These numbers agree with the following Eulerian formula for any facet $z_2 \in Z_2$,

$$m_V(\overset{\circ}{z}_2) - m_E(\overset{\circ}{z}_2) + m_P(z_2) = 1. \tag{10}$$

Formula (10) follows from an application of Euler's planar-graph formula to yield $m_V(z_2) - m_E(z_2) + m_P(z_2) = 1$, combined with $m_V(\partial z_2) = m_E(\partial z_2)$, for all $z_2 \in Z_2$.

Along each of the 10 edge-interiors mentioned above, the two coplanar plates of z_2 which meet along the edge make a dihedral angle equal to π and, at the three vertices in z_2's interior, all emanating edges are contained in a closed hemisphere centred on the vertex.

Definition 5. *An edge whose interior is contained in the interior of a facet is called a π-edge; the class of π-edges is $E[\pi]$. A vertex contained in the interior of a facet is called a hemi-vertex (and the class called $V[h]$). The proportion of π-edges in the tessellation is denoted by $\xi := \mu_{\overset{\circ}{E}\overset{\circ}{Z}_2}$ and the proportion of hemi-vertices by $\kappa := \mu_{V\overset{\circ}{Z}_2}$.*

There are 8 other cells positioned above z_2 which share a plate of this facet with the cell below z_2; two of these are shown in Figure 3(b) and we note that their facets extend beyond the shared plates. The triangular prism seen in (c) packs between the two cells of (b) and has one of its ridges lying along two collinear edges of our facet

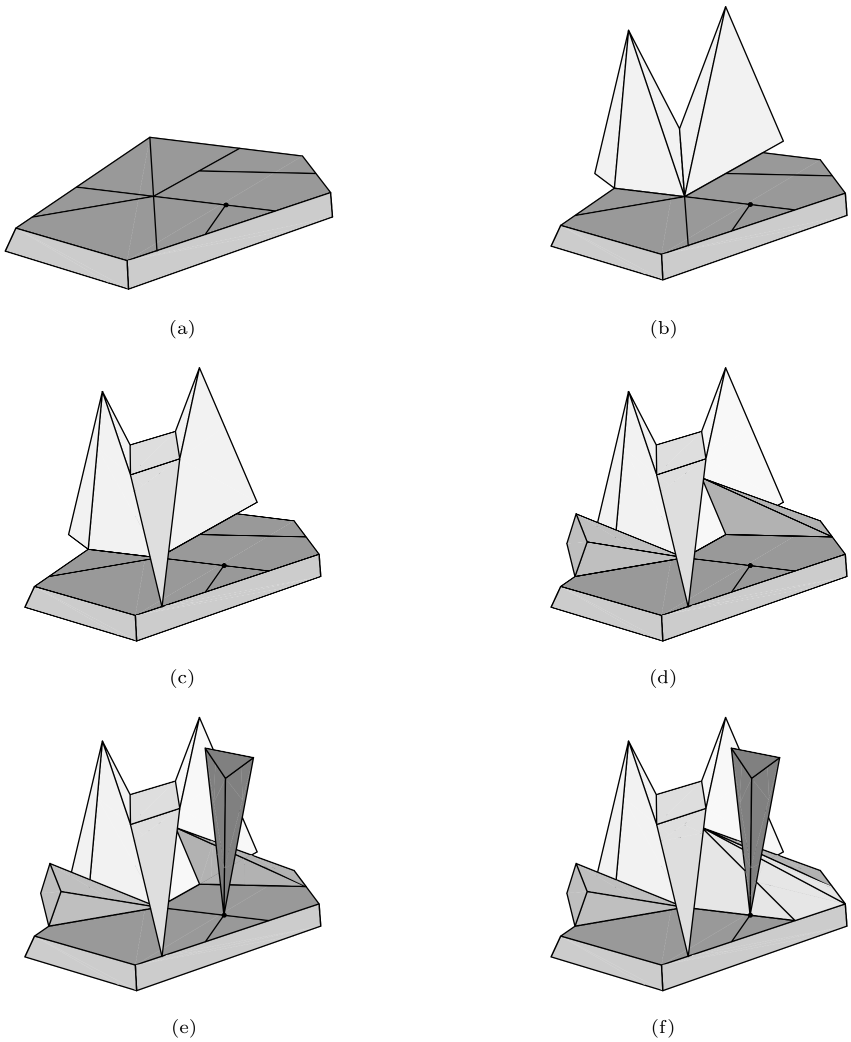

FIGURE 3: A cell facet $z_2 \in Z_2$ and some neighbouring cells. The cell positioned below z_2 has z_2 as one of its facets.

(seen in (a)).

Two other "above-cells" which share a plate with the cell below are shown in (d), whilst (e) shows a cell (the tall dark one) whose only contact with our facet z_2 is via one of its apices; the apex coincides with an interior-vertex of z_2. Yet another cell packs in behind the tall dark one in (f) – and there are other cells (not drawn) which fill the foreground.

From (10), we can derive λ_{Z_2}, the intensity of facets.

$$\mu_{\mathring{Z}_2 V} - \mu_{\mathring{Z}_2 \mathring{E}} + \mu_{Z_2 P} = 1.$$

Therefore

$$\begin{aligned}
\lambda_{Z_2} &= \lambda_{Z_2}\mu_{\mathring{Z}_2 V} - \lambda_{Z_2}\mu_{\mathring{Z}_2 \mathring{E}} + \lambda_{Z_2}\mu_{Z_2 P} \\
&= \lambda_V \mu_{V \mathring{Z}_2} - \lambda_E \mu_{\mathring{E}\mathring{Z}_2} + \lambda_P \mu_{P Z_2} && \text{using (5) and } \lambda_{\mathring{E}} = \lambda_E \\
&= \kappa\lambda_V - \xi\lambda_E + 2\lambda_P && \text{because } \mu_{P Z_2} = 2 \\
&= \big(\kappa - \tfrac{1}{2}\xi\ \mu_{VE} + \frac{\mu_{VE}\ \mu_{EP}}{\mu_{PV}}\big)\lambda_V && \text{from Table 2.} \qquad (11)
\end{aligned}$$

Furthermore, since λ_{Z_2} can also be written as $\lambda_Z \nu_2(Z)$, we can derive $\nu_2(Z)$, the expected number of faces of the typical cell.

$$\begin{aligned}
\nu_2(Z) &= \frac{\lambda_{Z_2}}{\lambda_Z} \\
&= \frac{2\kappa\ \mu_{PV} - \xi\ \mu_{VE}\ \mu_{PV} + 2\mu_{VE}\ \mu_{EP}}{f(\mu_{PV})} && \text{from (11) and Table 2} \\
&= \mu_{ZP} - \mu_{PV}\ \frac{\xi\ \mu_{VE} - 2\kappa}{f(\mu_{PV})}. && (12)
\end{aligned}$$

This is our first formula which is analogous to Cowan's planar formula (8). Other analogies, formula for $\nu_1(Z)$ and $\nu_0(Z)$, follow in the next section.

6. Description of ridges in a spatial tessellation

Figure 4(a) shows two facets of a cell, each containing some edges. These edges create three vertices on the ridge which is common to the two facets.

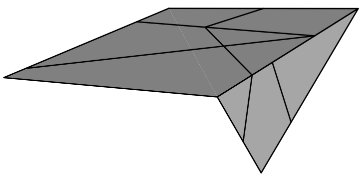

(a)

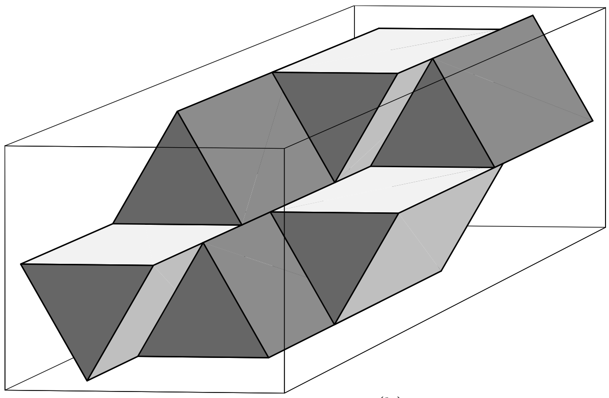

(b)

FIGURE 4: (a) Two facets of a cell and the ridge which is their intersection. (b) Six cells from a tessellation formed by congruent triangular prisms. The vertical axis is the z-axis, whilst the horizontal axes are the x-axis (pointing right) and the y-axis (pointing to the back).

There may, however, be other vertices in the ridge interior. For example, another cell may have an apex on the ridge. Or it might have one of its ridges intersecting with the ridge, creating one or two vertices additional to those shown in the figure.

So we must recognise that a vertex of the tessellation may lie in a ridge-interior (or indeed in many ridge interiors). This is true even for hemi-vertices. The expected number of ridge-interiors adjacent to a typical vertex, $\psi := \mu_{V\overset{\circ}{Z}_1}$, turns out to be an important parameter of spatial tessellations.

Example 1. *Consider Figure 4(b). Both triangular end-facets of the prism are equilateral triangles of side-length equal to* 1*. These facets are parallel to each other and to the* xz*-plane. They are orthogonal to the other three facets (which are* $1 \times L$ *rectangles). The tessellation is made up of cells of this type. The cells are packed around a central axis which is orthogonal to the* xz*-plane (and so parallel to the horizontal* y*-axis), thereby forming an infinite-length hexagonal rod. The rods pack to fill* $\mathbb{R}^3$*.*

The positioning of cells is such that whenever the xz*-plane cuts a cell, the distance between the cell's front* *triangular facet and the xz-plane is uniformly distributed in* $(0, L)$*, independently for each cell which is cut. (The origin* O *is uniformly distributed within one such cell.) So triangular facets (which always comprise one whole plate) never share an edge. The edges of the triangles are* π*-edges; there is one of these* π*-edges lying against each rectangular facet, dividing the facet into two rectangular plates. Every vertex is adjacent to* 5 *ridge-interiors, so* $\psi = 5$.

In order to find $\nu_1(Z)$, we note that

$$\mu_{Z_1 E} - \mu_{\overset{\circ}{Z}_1 V} = 1.$$

Therefore, using

$$\lambda_{Z_1} \mu_{Z_1 E} = \lambda_E(\mu_{EP} - \xi) \tag{13}$$

together with Table 2, (5) and $\lambda_{\overset{\circ}{Z}_1} = \lambda_{Z_1}$,

$$\begin{aligned} \lambda_{Z_1} &= \lambda_{Z_1}\mu_{Z_1 E} - \lambda_{\overset{\circ}{Z}_1}\mu_{\overset{\circ}{Z}_1 V} \\ &= \lambda_E(\mu_{EP} - \xi) - \lambda_V \mu_{V \overset{\circ}{Z}_1} \\ &= \tfrac{1}{2}\big(\mu_{VE}(\mu_{EP} - \xi) - 2\psi\big)\lambda_V. \end{aligned} \tag{14}$$

Because λ_{Z_1} also equals $\lambda_Z \nu_1(Z)$, Table 2 gives us:

$$\nu_1(Z) = \frac{\lambda_{Z_1}}{\lambda_Z} = \frac{\mu_{PV}(\mu_{VE}(\mu_{EP} - \xi) - 2\psi)}{f(\mu_{PV})} = \mu_{ZE} - \mu_{PV}\ \frac{\xi\ \mu_{VE} + 2\psi}{f(\mu_{PV})}. \tag{15}$$

So, from Euler's polyhedral formula, supplemented by (12), (15) and the caption of Table 2,

$$\nu_0(Z) = \nu_1(Z) - \nu_2(Z) + 2 = 2\ \mu_{PV}\ \frac{\mu_{VZ} - (\kappa + \psi)}{f(\mu_{PV})} = \mu_{ZV} - \mu_{PV}\ \frac{2(\kappa + \psi)}{f(\mu_{PV})}. \tag{16}$$

Therefore

$$\lambda_{Z_0} = \lambda_Z \nu_0(Z) = (\mu_{VZ} - \kappa - \psi)\lambda_V. \tag{17}$$

Every ridge is the side of two facets. So

$$\lambda_{(Z_2)_1} = 2\lambda_{Z_1} \tag{18}$$

$$\begin{aligned} \mu_{(Z_2)_1 E} &= \mu_{Z_1 E} \\ &= \frac{\lambda_E}{\lambda_{Z_1}}(\mu_{EP} - \xi) \qquad \text{from (13).} \end{aligned} \tag{19}$$

The identity (18) yields formulae for $\nu_1(Z_2)$ and $\nu_0(Z_2)$, the expected numbers of sides and corners of the typical facet. Trivially, $\lambda_{Z_2}\nu_1(Z_2) = \lambda_{(Z_2)_1}$. Therefore, using (14) and (11),

$$\nu_1(Z_2) = \frac{2\ \lambda_{Z_1}}{\lambda_{Z_2}} = \frac{2\ \mu_{PV}(\mu_{VE}(\mu_{EP} - \xi) - 2\psi)}{2\mu_{VE}\mu_{EP} - \mu_{PV}(\xi\mu_{VE} - 2\kappa)}. \tag{20}$$

Obviously, $\nu_0(Z_2) = \nu_1(Z_2)$.

7. Sides and corners of the typical plate

Following the methods employed above, we note that

$$\mu_{P_1 E} - \mu_{\overset{\circ}{P}_1 V} = 1.$$

So, using Table 2 and $\mu_{EP_1} = \mu_{EP}$,

$$\begin{aligned}\lambda_{P_1} =& \lambda_{P1}\mu_{P_1E} - \lambda_{P_1}\mu_{\overset{\circ}{P_1}V} \\ &= \lambda_E\mu_{EP_1} - \lambda_V\mu_{V\overset{\circ}{P_1}} \\ &= \tfrac{1}{2}\lambda_V(\mu_{VE}\mu_{EP} - 2\mu_{V\overset{\circ}{P_1}}).\end{aligned} \tag{21}$$

Therefore

$$\nu_1(P) = \frac{\lambda_{P_1}}{\lambda_P} = \mu_{PV}\ \frac{\mu_{VE}\ \mu_{EP} - 2\mu_{V\overset{\circ}{P_1}}}{\mu_{VE}\mu_{EP}} = \mu_{PV}\big(1 - \frac{2\tau}{\mu_{VE}\mu_{EP}}\big), \tag{22}$$

where $\tau := \mu_{V\overset{\circ}{P_1}}$, the expected number of plate-side interiors adjacent to a typical vertex. In the prism tessellation, $\tau = 4$. Obviously $\nu_0(P) = \nu_1(P)$.

Every plate $p \in P$ is contained in two cells, z and z' say. It lies in a facet of each, say z_2 of z and z_2' of z'. Consider a side p_1 of p and suppose there exists a vertex $v \subset \overset{\circ}{p}_1$. If v is not a hemi-vertex of the tessellation, then

(a) $\overset{\circ}{p}_1$ is contained in a ridge of z and also in a ridge of z' – as is v.

If v is a hemi-vertex, then either (a) is true or

(b) $\overset{\circ}{p}_1$ is contained in a ridge of one of the cells, z or z', and in the interior of a facet of the other cell – as is v.

8. $\boldsymbol{\lambda_X, \nu_j(X)}$ and $\boldsymbol{\mu_{XY}}$ and in the spatial case

Using the abbreviation f, defined in (6), together with

$$t(x) := 2\mu_{VE}\mu_{EP} - x(\xi\mu_{VE} - 2\kappa), \tag{23}$$

we express $\nu_j(X)$, and the remaining λ_X in tabular form.

X	λ_X/λ_V
facets Z_2	$\dfrac{t(\mu_{PV})}{2\mu_{PV}}$
ridges Z_1	$\frac{1}{2}(\mu_{VE}(\mu_{EP} - \xi) - 2\psi)$
apices Z_0	$\frac{1}{2}f(2) - \kappa - \psi$
facet-sides $(Z_2)_1$	$\mu_{VE}(\mu_{EP} - \xi) - 2\psi$
facet-corners $(Z_2)_0$	$\mu_{VE}(\mu_{EP} - \xi) - 2\psi$
plate-sides P_1	$\frac{1}{2}(\mu_{VE}\mu_{EP} - 2\tau)$
plate-corners P_0	$\frac{1}{2}(\mu_{VE}\mu_{EP} - 2\tau)$
edge-termini E_0	μ_{VE}
ridge-termini $(Z_1)_0$	$\mu_{VE}(\mu_{EP} - \xi) - 2\psi$
plate-side-termini $(P_1)_0$	$\mu_{VE}\mu_{EP} - 2\tau$
facet-side-termini $((Z_2)_1)_0$	$2(\mu_{VE}(\mu_{EP} - \xi) - 2\psi)$

Table 5: Intensities for non-primitives in spatial tessellations, from (11), (14), (17), (18), (21) and (23).

X	$\nu_0(X)$	$\nu_1(X)$	$\nu_2(X)$
E	2	-	-
Z_1	2	-	-
P_1	2	-	-
$(Z_2)_1$	2	-	-
P	$\mu_{PV}\Big(1-\dfrac{2\tau}{\mu_{VE}\mu_{EP}}\Big)$	$\mu_{PV}\Big(1-\dfrac{2\tau}{\mu_{VE}\mu_{EP}}\Big)$	-
Z_2	$2\dfrac{\mu_{VE}(\mu_{EP}-\xi)-2\psi}{t(\mu_{PV})\ (\mu_{PV})^{-1}}$	$2\dfrac{\mu_{VE}(\mu_{EP}-\xi)-2\psi}{t(\mu_{PV})\ (\mu_{PV})^{-1}}$	-
Z	$\mu_{ZV}-\mu_{PV}\dfrac{2(\kappa+\psi)}{f(\mu_{PV})}$	$\mu_{ZE}-\mu_{PV}\dfrac{\xi\mu_{VE}+2\psi}{f(\mu_{PV})}$	$\mu_{ZP}-\mu_{PV}\dfrac{\xi\mu_{VE}-2\kappa}{f(\mu_{PV})}$

Table 6: Values of $\nu_j(X),\ j\leq 2$, from (22), (20), (12), (15), (16) and (23).

We also tabulate, in Table 7, some additional μ_{XY} formulae (supplementing Table 2). Tables 2 and 7 contain all μ-values which can be expressed in terms of our three cyclic *mean adjacencies* parameters, μ_{VE}, μ_{EP} and μ_{PV}, and our four Greek parameters ξ, κ, ψ and τ.

μ	V	E	P	Z
Z_2	$2\mu_{PV}\dfrac{\kappa+\mu_{VE}(\mu_{EP}-\xi)}{t(\mu_{PV})}$	$\mu_{PV}\dfrac{\mu_{VE}(2\mu_{EP}-\xi)}{t(\mu_{PV})}$	$\dfrac{2\mu_{VE}\mu_{EP}}{t(\mu_{PV})}$	-
Z_1	$2\dfrac{\mu_{VE}(\mu_{EP}-\xi)-\psi}{\mu_{VE}(\mu_{EP}-\xi)-2\psi}$	$\dfrac{\mu_{VE}(\mu_{EP}-\xi)}{\mu_{VE}(\mu_{EP}-\xi)-2\psi}$	-	-
$(Z_2)_1$	$2\dfrac{\mu_{VE}(\mu_{EP}-\xi)-\psi}{\mu_{VE}(\mu_{EP}-\xi)-2\psi}$	$\dfrac{\mu_{VE}(\mu_{EP}-\xi)}{\mu_{VE}(\mu_{EP}-\xi)-2\psi}$	-	-
P_1	$2\dfrac{\mu_{VE}\mu_{EP}-\tau}{\mu_{VE}\mu_{EP}-2\tau}$	$\dfrac{\mu_{VE}\mu_{EP}}{\mu_{VE}\mu_{EP}-2\tau}$	-	-

μ	Z_2	Z_1	$(Z_2)_1$	P_1
V	$\kappa+\mu_{VE}(\mu_{EP}-\xi)$	$\mu_{VE}(\mu_{EP}-\xi)-\psi$	$2(\mu_{VE}(\mu_{EP}-\xi)-\psi)$	$\mu_{VE}\mu_{EP}-\tau$
E	$2\mu_{EP}-\xi$	$\mu_{EP}-\xi$	$2(\mu_{EP}-\xi)$	μ_{EP}
P	2	-	-	-
Z	-	-	-	-

Table 7: Other values of μ_{XY}, where, either ... $x\in X \Rightarrow \dim(x)>0$ and $Y\in\{V,E,P,Z\}$ or ... $y\in Y\Rightarrow \dim(y)>0$ and $X\in\{V,E,P,Z\}$. Those entries marked "-" cannot be expressed in terms of the entities defined in this paper.

We refer the reader to Appendix B which provides techniques of proof for the results in Table 7, whilst also indicating methods to deal with non-primitive objects of dimension 0 (which have in their formulae various second moments, or sub-type first moments such as μ_{XY} where $X=E[\pi]$).

It is impractical to present a full 15×15 table comprising all μ_{XY} formulae, many of which are typographically lengthy. We turn instead to examples.

9. Application to three examples

We consider three examples: the spatial STIT model, which provides a three-dimensional version of Figure 2(a); a tetrahedral model; the prism tessellation illustrated in Figure 4(b).

The spatial STIT model: The μ-values for primitive elements in the spatial STIT model are known (from Nagel and Weiss [23]) and are tabulated below in Table 8(a). Using the values in Table 8(a), we can fill out our Table 6 with STIT results – see Table 8(b). A list of intensities is compiled in Table 8(c).

μ	V	E	P	Z
V	1	4	6	4
E	2	1	3	3
P	$\frac{36}{7}$	$\frac{36}{7}$	1	2
Z	24	36	14	1

(a)

X	$\nu_0(X)$	$\nu_1(X)$	$\nu_2(X)$
P	$\frac{6}{7}(6-\tau)$	$\frac{6}{7}(6-\tau)$	-
Z_2	$\dfrac{6(6-2\xi-\psi)}{3\kappa+1}$	$\dfrac{6(6-2\xi-\psi)}{3\kappa+1}$	-
Z	$24-6(\kappa+\psi)$	$36-6(2\xi+\psi)$	$14-6(2\xi-\kappa)$

(b)

X	V	E	P	Z	Z_2	Z_1	Z_0	$(Z_2)_1$	$(Z_2)_0$	P_1	P_0	X_0, $\dim X = 1$
λ_X/λ_V	1	2	$\frac{7}{6}$	$\frac{1}{6}$	1	2	$\frac{4}{3}$	4	4	$\frac{14}{3}$	$\frac{14}{3}$	$\lambda_{X_0} = 2\lambda_X$

(c)

Table 8: For the spatial STIT process: (a) adjacencies μ for the primitives; (b) ν-values; (c) intensities.

It is known that the interior of the typical cell of a spatial STIT model has the same distribution as the interior of the typical cell in a Poisson plane-process. So

$$\nu_0(Z) = 8, \quad \nu_1(Z) = 12, \quad \nu_2(Z) = 6.$$

This implies, from the last row of Table 8(b) and the fact obvious from the STIT construction that all edges are π-edges, that

$$\psi = 2, \quad \kappa = \frac{2}{3} \quad \text{and } \xi = 1. \tag{24}$$

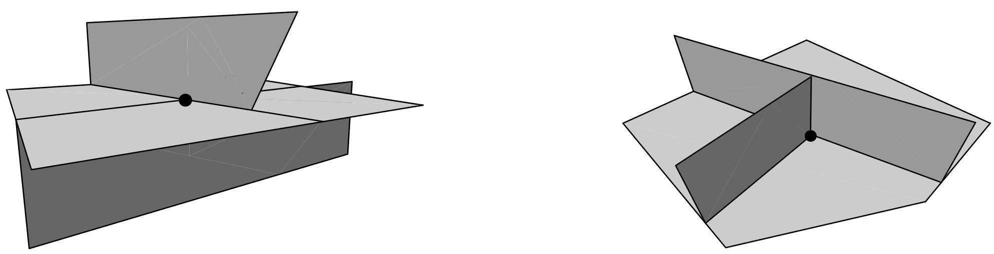

(a) (b)

FIGURE 5: (a) A *crossing vertex* in the STIT tessellation. (b) A *hemi-vertex* in the STIT tessellation.

These results for ψ and κ are new, arising from the theory of this paper. Also new is the result $\nu_0(Z_2) = \nu_1(Z_2) = 4$, proved using Table 8(b) and (24).

A spatial STIT tessellation has two types of vertex, illustrated in Figure 5. Type (a), which we call a *crossing* vertex, is adjacent to two plate-side-interiors and four ridge-interiors and no facet-interior. Type (b) is adjacent to one plate-side-interior, one ridge-interior and one facet-interior (which makes it a *hemi-vertex*). Because $\kappa = \frac{2}{3}$, the probabiliy that a typical vertex is *hemi-type* is $\frac{2}{3}$. So $\tau = 2\times\frac{1}{3}+1\times\frac{2}{3} = \frac{4}{3}$. We check that $\psi = 4\times\frac{1}{3}+1\times\frac{2}{3} = 2$, as derived above.

The first row of Table 8(b) now gives us $\nu_0(P) = \nu_1(P) = 4$. Interestingly, the typical plate has the same average number of sides as the typical facet. On average, a typical facet comprises $\mu_{Z_2P} = \frac{7}{3}$ plates – a result coming from Table 7, rewritten as Table 9 below:

μ	V	E	P	Z
Z_2	$\frac{26}{3}$	10	$\frac{7}{3}$	-
Z_1	3	2	-	-
$(Z_2)_1$	3	2	-	-
P_1	$\frac{16}{7}$	$\frac{9}{7}$	-	-

μ	Z_2	Z_1	$(Z_2)_1$	P_1
V	$\frac{26}{3}$	6	12	$\frac{32}{3}$
E	5	2	4	3
P	2	-	-	-
Z	-	-	-	-

Table 9: Various adjacencies for the spatial STIT model.

Remark 2. *All of the results for this STIT example were unknown prior to this study. Some of the results, however, have been computed in a study (see Thäle and Weiss [29]) conducted in parallel with our paper, using only properties of STIT tessellations. The original content in this section is shared with [29]; neither paper has priority over the other.*

A tetrahedral model: A spatial tessellation in which all cells are tetrahedra has $\nu_0(Z) = \nu_2(Z) = 4$ and $\nu_1(Z) = 6$. So two independent equations (in the six unknowns $\mu_{VE}, \mu_{EP}, \mu_{PV}, \xi, \kappa$ and ψ) can be found from the last row of Table 6, allowing us to express two of the variables in terms of the other four. Choosing κ and ψ, we have:

$$\kappa = 4 - \mu_{VE}\Big(2 - \tfrac{1}{2}\xi - \frac{\mu_{EP}}{\mu_{PV}}\Big); \tag{25}$$

$$\psi = \mu_{VE}\Big(3 + \tfrac{1}{2}(\mu_{EP} - \xi) - 3\frac{\mu_{EP}}{\mu_{PV}}\Big) - 6. \tag{26}$$

Reassuringly, these equations then prove that the expression in Table 6 for $\nu_0(Z_2)$ collapses to 3, as it should; facets of tetrahedra are triangles.

The best known example of a spatial tessellation comprising only tetrahedral cells is the Poisson-Delaunay tessellation. This is a *facet-to-facet* tessellation, so $\kappa = \xi = \psi = \tau = 0$ and $\mu_{PV} = 3$. It is also known, from [15], [19], [20] and [18] (see also [24]), that

$$\mu_{VE} = 2 + \frac{48\pi^2}{35} \approx 15.5355 \qquad \text{and} \qquad \mu_{EP} = \frac{144\pi^2}{24\pi^2 + 35} = 6 - \frac{12}{\mu_{VE}} \approx 5.2276. \tag{27}$$

Also:

$$\lambda_E = \Big(1 + \frac{24\pi^2}{35}\Big)\lambda_V; \qquad \lambda_P = \frac{48\pi^2}{35}\,\lambda_V; \qquad \lambda_Z = \frac{24\pi^2}{35}\,\lambda_V.$$

The equality in (27) of μ_{EP} and $6 - 12/\mu_{VE}$ is predicted by equations (25) and (26), one of which becomes redundant in this particular case.

We now construct a tetrahedral model which is not *facet-to-facet* – and we do this by randomly and independently dividing each cell of a Poisson-Delaunay tessellation into two tetrahedral cells. This is achieved by randomly choosing one of the 6 ridges of the tetrahedral cell (whose vertices we generically label $ABCD$, for discussion purposes, with AB the randomly chosen ridge) and a uniformly random point Q on the *opposite* ridge CD. Construct a dividing plane containing AB and Q, an exercise repeated for all cells.

Because each cell divides, the new λ_Z (denoted with $'$) is

$$\lambda'_Z = 2\ \lambda_Z.$$

The new dividing plane ABQ in our generic cell creates two lines, AQ on the original plate ACD and BQ on the original plate BCD. Focussing on the original plate ACD, we note that it may acquire another line (with one end placed at either A, C or D) through the division of the *other* cell adjacent to ACD – and this line might cross the line AQ forming a vertex of *crossing type* (see Figure 5(a)). The original plate ACD will become, post-division, one of the following structures.

- ACD becomes four plates, three being triangular and one four-sided, because of the creation of a crossing-type vertex. The new lines have also created four π-edges. This outcome has probability $\frac{1}{6}$.
- It remains untouched by new lines, with probability $\frac{1}{4}$.
- Just one of its adjacent cells places a line on ACD (probability $\frac{1}{2}$), creating one π-edge and dividing the plate ACD into two triangular plates.
- Two non-crossing lines are created on ACD (probability $\frac{1}{12}$), dividing ACD into three triangular plates and adding two π-edges to the tessellation.

Each of the new π-edges mentioned above is adjacent to three plates.

Accounting for these outcomes, we can write (using $P[j]$ to denote the class of plates with j sides):

$$\begin{aligned}
\lambda'_P &= \lambda_Z + \lambda_P\Big(\tfrac{1}{6}\times 4 + \tfrac{1}{4}\times 1 + \tfrac{1}{2}\times 2 + \tfrac{1}{12}\times 3\Big) = \frac{128\pi^2}{35}\ \lambda_V;\\
\lambda'_{P[4]} &= \tfrac{1}{6}\ \lambda_P = \frac{8\pi^2}{35}\ \lambda_V;\\
\lambda'_{P[3]} &= \lambda'_P - \lambda'_{P[4]} = \frac{120\pi^2}{35}\ \lambda_V;\\
\nu'_0(P) = \nu'_1(P) &= \frac{3\lambda'_{P[3]} + 4\lambda'_{P[4]}}{\lambda'_P} = \frac{49}{16} \approx 3.0625;\\
\lambda'_{E[\pi]} &= \lambda_P\Big(\tfrac{1}{6}\times 4 + \tfrac{1}{4}\times 0 + \tfrac{1}{2}\times 1 + \tfrac{1}{12}\times 2\Big) = \frac{64\pi^2}{35}\ \lambda_V.
\end{aligned} \tag{28}$$

Prior to the division, an edge e was adjacent to $m_P(e)$ plates and $m_Z(e)$ cells; here $m_P(e) = m_Z(e)$ due to the facet-to-facet property of the Poisson-Delaunay tessellation. After division, e has been split into a random number R of non-π edges $e_1, e_2, ..., e_R$ by various generic Q-points. Edge e_i is adjacent post-division to a random number $m'_P(e_i)$ of plates. Clearly $\mathsf{E}(R|m_Z(e)) = 1 + \frac{1}{6}m_Z(e)$ because each of the $m_Z(e)$ cells originally adjacent to e will place its Q-point on e with probability $\frac{1}{6}$. Also $\mathsf{E}(m'_P(e_i)|m_Z(e), m_P(e)) = m_P(e) + \frac{1}{6}m_Z(e) = \frac{7}{6}m_P(e)$, for all i; this follows because each of these $m_Z(e)$ cells will select e as its AB-ridge with probability $\frac{1}{6}$.

Therefore, using $E[\overline{\pi}]$ to denote the class of non-π edges, we have:

$$\lambda'_{E[\overline{\pi}]} = \left(1 + \tfrac{1}{6}\ \mu_{EZ}\right)\ \lambda_E = \left(1 + \tfrac{1}{6}\ \mu_{EP}\right)\ \lambda_E = \left(1 + \frac{48\pi^2}{35}\right)\lambda_V;$$

$$\lambda'_E = \lambda'_{E[\pi]} + \lambda'_{E[\overline{\pi}]} = \left(1 + \frac{16\pi^2}{5}\right)\ \lambda_V;$$

$$\xi' = \frac{\lambda'_{E[\pi]}}{\lambda'_E} = \frac{64\pi^2}{7(5+16\pi^2)} \approx 0.5539; \tag{29}$$

$$\mu'_{EP} = 3\xi' + \tfrac{7}{6}\ \mu_{EP}(1-\xi') = \frac{72\pi^2(175+176\pi^2)}{7(5+16\pi^2)(35+24\pi^2)} \approx 4.3824. \tag{30}$$

Additionally,

$$\lambda'_V = \lambda_V + \tfrac{1}{6}\ \lambda_P + \tfrac{1}{6}\ \mu_{EZ}\ \lambda_E = \left(1 + \frac{32\pi^2}{35}\right)\ \lambda_V,$$

with the three types – original, crossing-type and Q-point vertex – being in proportions $35 : 8\pi^2 : 24\pi^2$. The latter two types have $m_E(v) = 4$ whilst $\mathsf{E}(m_E(v)|v \text{ is original}) = \mu_{VE} + \frac{1}{2}\mu_{VZ}$. Therefore,

$$\mu'_{VE} = \frac{35 \times (\mu_{VE} + \frac{1}{2}\mu_{VZ}) + (8+24)\pi^2 \times 4}{35+32\pi^2} = \frac{14(5+16\pi^2)}{35+32\pi^2} \approx 6.5012, \tag{31}$$

using $\mu_{VZ} = \frac{1}{2}f(2) = \frac{1}{2}\mu_{VE}\mu_{EP} - \mu_{VE} + 2 = 96\pi^2/35$.

Equations (29)–(31) give us three of the seven fundamental parameters; these, combined with the obvious result, $\kappa' = 0$, enables us to solve (25) for μ_{PV}, obtaining

$$\mu'_{PV} = \frac{9(175+176\pi^2)}{16(35+24\pi^2)} \approx 3.9560. \tag{32}$$

Now solving (26) for ψ yields

$$\psi' = \frac{8\pi^2(35+528\pi^2)}{(35+24\pi^2)(35+32\pi^2)} \approx 4.3429. \tag{33}$$

Finally, the seventh and last fundamental parameter, τ', is found from Table 6 combined with (30)–(32) and (28).

$$\tau' = \tfrac{1}{2}\mu'_{VE}\mu'_{EP}\left(1 - \frac{\nu'_0(P)}{\mu'_{PV}}\right) = \frac{32\pi^2(102\pi^2-35)}{(35+24\pi^2)(35+32\pi^2)} \approx 3.2176. \tag{34}$$

All seven parameters are now in place, $\kappa' = 0$ and those displayed as (29)–(34).

The triangular-prism example (Example 1 continued): As this fairly regular tessellation can be visualised clearly in Figure 4(b), equation (35) and the entries in the following tables are presented without further comment.

$$\xi = \frac{1}{2}, \qquad \kappa = 0, \qquad \psi = 5 \qquad \text{and } \tau = 4. \tag{35}$$

μ	V	E	P	Z
V	1	4	9	7
E	2	1	$\frac{9}{2}$	$\frac{9}{2}$
P	$\frac{27}{4}$	$\frac{27}{4}$	1	2
Z	21	27	8	1

X	$\nu_0(X)$	$\nu_1(X)$	$\nu_2(X)$
P	$\frac{15}{4}$	$\frac{15}{4}$	-
Z_2	$\frac{18}{5}$	$\frac{18}{5}$	-
Z	6	9	5

X	E	P	Z	Z_2	Z_1	Z_0	$(Z_2)_1$	$(Z_2)_0$	P_1	P_0	X_0, $\dim X = 1$
λ_X/λ_V	2	$\frac{4}{3}$	$\frac{1}{3}$	$\frac{5}{3}$	3	2	6	6	5	5	$\lambda_{X_0} = 2\lambda_X$

μ	V	E	P	Z
Z_2	$\frac{48}{5}$	$\frac{51}{5}$	$\frac{8}{5}$	-
Z_1	$\frac{11}{3}$	$\frac{8}{3}$	-	-
$(Z_2)_1$	$\frac{11}{3}$	$\frac{8}{3}$	-	-
P_1	$\frac{14}{5}$	$\frac{9}{5}$	-	-

μ	Z_2	Z_1	$(Z_2)_1$	P_1
V	16	11	22	14
E	$\frac{17}{2}$	4	8	$\frac{9}{2}$
P	2	-	-	-
Z	-	-	-	-

Table 10: Various parameters in the triangular-prism tessellation.

10. Concluding remarks

For spatial tessellations, we have introduced seven fundamental parameters. These are the three *mean adjacencies* μ_{VE}, μ_{EP} and μ_{PV} which are sufficient to describe the more important topological relationships in facet-to-facet tessellations, and our four Greek parameters ξ, κ, ψ and τ which are needed in other cases. The constraints which apply to these seven parameters are complicated. So we defer the study of the seven-dimensional parameter-space to a later paper.

We note that, even in the simpler facet-to-facet case, no study of the constraints operative on μ_{VE}, μ_{EP} and μ_{PV} has yet been published by other authors.

Appendix A: The planar adjacencies in Table 4

Lemma 1. *If a vertex $v \in V$ is adjacent to $m_E(v)$ edges and $m_{Z_1}^{\circ}(v)$ side-interiors, then it is adjacent to:*

$(m_E(v) - m_{Z_1}^{\circ}(v))$ corners; $(2m_E(v) - m_{Z_1}^{\circ}(v))$ sides; $m_E(v)$ cells;

$m_E(v)$ edge-termini; $2(m_E(v) - m_{Z_1}^{\circ}(v))$ side-termini.

Note that $m_{Z_1}^{\circ}(v)$ equals either 1 or 0, the vertex v being a π-vertex or not respectively.

This obvious Lemma immediately gives us μ_{VY} for any object-class Y in the tessellation– and this leads to μ_{YV} via (5). For example, when Y is the class Z_1 of cell-sides,

$$\mu_{VZ_1} = \mathsf{E}_V m_{Z_1}(v) = \mathsf{E}_V(2m_E(v) - m_{Z_1}^{\circ}(v)) = 2\mu_{VE} - \mu_{VZ_1^{\circ}} = 2\mu_{VE} - \phi.$$

Therefore

$$\mu_{Z_1V} = \frac{\lambda_V}{\lambda_{Z_1}}\ \mu_{VZ_1} = \frac{2\mu_{VE} - \phi}{\mu_{VE} - \phi}.$$

Objects of dimension 0 lie on the vertices of the tessellation. If X is a class of 0-dimensional objects, that is $X \in \{V, E_0, Z_0, (Z_1)_0\}$, its point process can be viewed as a marked point process: a process of points located at the vertices with a mark at a vertex v of $m_X(v)$. So it is easily seen that, for any object-class Y in the tessellation,

$$\lambda_X \mu_{XY} = \lambda_V \mathsf{E}_V(m_X(v) m_Y(v)). \tag{36}$$

This identity, combined with Lemma 1, provides us with most of the formulae in Table 4. For example, if X is the class Z_0 of corners and Y is the class Z_1 of sides,

$$\begin{aligned}
\mu_{Z_0Z_1} &= \frac{\lambda_V}{\lambda_{Z_0}}\ \mathsf{E}_V(m_{Z_0}(v)m_{Z_1}(v)) \\
&= \frac{1}{\mu_{VE}-\phi}\ \mathsf{E}_V[(m_E(v)-m^{\circ}_{Z_1}(v))(2m_E(v)-m^{\circ}_{Z_1}(v))] \\
&= \frac{1}{\mu_{VE}-\phi}\ \mathsf{E}_V[2m_E(v)^2-3m_E(v)m^{\circ}_{Z_1}(v)+(m^{\circ}_{Z_1}(v))^2] \\
&= \frac{2\mu^{(2)}_{VE}-3\phi\ \mu_{V[\pi]E}+\phi}{\mu_{VE}-\phi},
\end{aligned}$$

using the fact that $(m^{\circ}_{Z_1}(v))^2 = m^{\circ}_{Z_1}(v)$ (see Lemma 1) and:

$$\begin{aligned}
\mathsf{E}_V(m^{\circ}_{Z_1}(v)) &= \phi\mathsf{E}_V(m^{\circ}_{Z_1}(v)|m^{\circ}_{Z_1}(v)=1) = \phi\ ; \\
\mathsf{E}_V(m_E(v)m^{\circ}_{Z_1}(v)) &= \phi\mathsf{E}_V(m_E(v)m^{\circ}_{Z_1}(v)|m^{\circ}_{Z_1}(v)=1) \\
&= \phi\mathsf{E}_V(m_E(v)|m^{\circ}_{Z_1}(v)=1) = \phi\mu_{V[\pi]E}.
\end{aligned}$$

The remaining formulae in Table 4 follow either from the use of (5) or by very simple arguments which we leave to the reader.

Appendix B: The spatial adjacencies

Objects of dimension 0: In the spatial case also, objects of dimension 0 lie on the vertices of the tessellation. So the mathematical approach to adjacency relationships such as μ_{XY} when the objects $\in X$ all have dimension 0 follows the same style as in the planar case. In the spatial case, however, Lemma 2 replaces Lemma 1.

Lemma 2. *If a vertex v is adjacent to $m_E(v)$ edges, $m_{E[\pi]}(v)$ π-edges, $m_P(v)$ plates, $m^{\circ}_{Z_2}(v)$ facet-interiors, $m^{\circ}_{Z_1}(v)$ ridge-interiors and $m^{\circ}_{P_1}(v)$ plate-side-interiors, then it is adjacent to:*

$(m_P(v)-m_E(v)+2)$ cells;	$m_E(v)$ edge-termini;
$(m^{\circ}_{Z_2}(v)+2m_P(v)-m_{E[\pi]}(v))$ facets;	$2(2m_P(v)-m_{E[\pi]}(v)-m^{\circ}_{Z_1}(v))$ facet-sides;
$(2m_P(v)-m_{E[\pi]}(v)-m^{\circ}_{Z_1}(v))$ ridges;	$2(m_P(v)-m^{\circ}_{P_1}(v))$ plate-side-termini;
$(2m_P(v)-m^{\circ}_{P_1}(v))$ plate-sides;	$(m_P(v)-m^{\circ}_{P_1}(v))$ plate-corners;
$(2m_P(v)-m_{E[\pi]}(v)-2m^{\circ}_{Z_1}(v))$ ridge-termini;	$(2m_P(v)-m_{E[\pi]}(v)-2m^{\circ}_{Z_1}(v))$ facet-corners;
$2(2m_P(v)-m_{E[\pi]}(v)-2m^{\circ}_{Z_1}(v))$ facet-side-termini;	$(m_P(v)-m_E(v)+2-m^{\circ}_{Z_2}(v)-m^{\circ}_{Z_1}(v))$ apices.

Note that $m^{\circ}_{Z_2}(v)$ equals either 1 or 0, the vertex being a hemi-vertex or not respectively.

This Lemma gives us μ_{VY} for any object Y in the tessellation. For example, when Y is a facet-side $(Z_2)_1$,

$$\begin{aligned}
\mu_{V(Z_2)_1} = \mathsf{E}_V(m_{(Z_2)_1}(v)) &= 2\mathsf{E}_V(2m_P(v)-m_{E[\pi]}(v)-m^{\circ}_{Z_1}(v)) \\
&= 2(2\mu_{VP}-\mu_{VE[\pi]}-\psi) \\
&= 2(\mu_{VE}(\mu_{EP}-\xi)-\psi).
\end{aligned}$$

For $X \in \{V, E_0, P_0, Z_0, (Z_1)_0, (Z_2)_0, (P_1)_0, ((Z_2)_1)_0\}$, we can use (36) to establish μ_{XY}. For example, if X is the class $(P_1)_0$ of plate-side-termini and Y is the class of Z_2 facets, then

$$\begin{aligned}
\mu_{(P_1)_0 Z_2} &= \frac{\lambda_V}{\lambda_{(P_1)_0}}\ \mathsf{E}_V(m_{(P_1)_0}(v) m_{Z_2}(v)) \\
&= \frac{1}{\mu_{VE}\mu_{EP} - 2\tau}\ \mathsf{E}_V[2(m_P(v) - m^{\circ}_{P_1}(v))(m^{\circ}_{Z_2}(v) + 2m_P(v) - m_{E[\pi]}(v))] \\
&= \frac{2}{\mu_{VE}\mu_{EP} - 2\tau}\ \Big[\mathsf{E}_V(m_P(v) m^{\circ}_{Z_2}(v)) + 2\mu^{(2)}_{VP} - \mathsf{E}_V(m_P(v) m_{E[\pi]}(v)) \\
&\qquad - \mathsf{E}_V(m^{\circ}_{P_1}(v) m^{\circ}_{Z_2}(v)) - 2\mathsf{E}_V(m^{\circ}_{P_1}(v) m_P(v)) \\
&\qquad\quad + \mathsf{E}_V(m^{\circ}_{P_1}(v) m_{E[\pi]}(v))\Big] \\
&= \frac{2}{\mu_{VE}\mu_{EP} - 2\tau}\Big[\psi\mu_{V[h]P} + 2\mu^{(2)}_{VP} - \mathsf{E}_V(m_P(v) m_{E[\pi]}(v)) \\
&\qquad - \psi\mu_{V[h]P^{\circ}_1} - 2\mathsf{E}_V(m^{\circ}_{P_1}(v) m_P(v)) + \mathsf{E}_V(m^{\circ}_{P_1}(v) m_{E[\pi]}(v))\Big].
\end{aligned}$$

We see that expressions can be quite expansive typographically and involve many second moments.

Obviously, all examples of μ_{XY} with Y having dimension 0 can be calculated by first finding μ_{YX} and then using (5).

Objects of dimension 1**:** The following lemma establishes the adjacencies μ_{XY} (and μ_{YX}) in Table 7, when Y comprises objects of dimension ≥ 1 and $X = E$.

Lemma 3. *If an edge $e \in E$ is adjacent to $m_P(e)$ plates and $m^{\circ}_{Z_2}(e)$ facet-interiors, then it is adjacent to:*

$(m_P(e) - m^{\circ}_{Z_2}(e))$ ridges; $(2m_P(e) - m^{\circ}_{Z_2}(e))$ facets; $m_P(e)$ cells;

$m_P(e)$ plate-sides; $2(m_P(e) - m^{\circ}_{Z_2}(e))$ facet-sides.

Note that $m^{\circ}_{Z_2}(e)$ equals either 1 *or* 0*, the edge being a π-edge or not respectively.*

For example, $\mu_{EZ_2} = \mathsf{E}_E(m_{Z_2}(e)) = \mathsf{E}_E(2m_P(e) - m^{\circ}_{Z_2}(e)) = 2\mu_{EP} - \xi$. Then, by using (5),

$$\mu_{Z_2 E} = \frac{\lambda_E}{\lambda_{Z_2}}\mu_{EZ_2} = \frac{\mu_{VE}\mu_{PV}}{t(\mu_{PV})}(2\mu_{EP} - \xi) = \frac{\mu_{PV}}{t(\mu_{PV})}\ \mu_{VE}(2\mu_{EP} - \xi).$$

Higher dimensional objects: Formulae for μ_{XY} when $\dim(Y) \geq \dim(X) \geq 2$ are more difficult to address. They cannot be expressed in terms of the parameters we have introduced, so they lie outside the scope of this paper.

References

[1] Arak, T., Clifford, P. and Surgailis, D. (1993) Point-based polygonal models for random graphs. *Adv. Appl. Prob.* **25**, 348–372.

[2] Cowan, R. (1978). The use of ergodic theorems in random geometry. *Suppl. Adv. Appl. Prob.* **10,** 47–57.

[3] Cowan, R. (1980). Properties of ergodic random mosaic processes. *Math. Nachr.* **97,** 89–102.

[4] Cowan, R. and Morris, V. B. (1988). Division Rules for Polygonal Cells. *J. theor. Biol.* **131,** 33–42.

[5] Cowan, R. (2004). A mosaic of triangular cells formed with sequential splitting rules. *Stochastic Methods and their Applications. J. Appl. Prob.* **41A**, 3–15.

[6] Cowan, R. (2010). New classes of random tessellations arising from iterative division of cells. *Adv. Appl. Prob.*, **42**, 26–47.

[7] Cowan, R. and Tsang, A. K. L. (1994). The falling-leaf mosaic and its equilibrium properties. *Adv. Appl. Prob.*, **26**, 54–62.

[8] Grünbaum, B. and Shephard, G. C. (1987). *Tilings and Patterns.* W, H, Freeman and Co., New York.

[9] Kendall, W. S. and Mecke, J. (1987). The range of mean-value quantities of planar tessellations. *J. Appl. Prob.*, **24**, 411–421.

[10] Leistritz, L. and Zähle, M. (1992). Topological Mean Value Relationships for Random Cell Complexes. *Math. Nachr.* **155**, 57–72.

[11] Mecke, J. (1980) Palm methods for stationary random mosaics. In *Combinatorial Principles in Stochastic Geometry,* ed. R.A. Ambartzumian. Armenian Academy of Science, Erevan.

[12] Mecke, J. (1983). Zufällige Mosaike. Chapter 8 of *Stochastische Geometrie.* Akademie-Verlag, Berlin.

[13] Mecke, J. (1984). Parametric representation of mean values for stationary random mosaics. *Math. Operations. Statist. Ser. Statist.* **15,** 437–442.

[14] Mecke, J., Nagel, W. and Weiss, V. (2007). Length distributions of edges in planar stationary and isotropic STIT tessellations. *Izvestija Akademii Nauk Armenii, Matematika.* **42**, 39–60.

[15] Miles, R. E. (1970). On the homogeneous planar Poisson point process. *Math. Biosciences.* **6**, 85–127.

[16] Miles, R. E. (1988). Matschinski's identity and dual random tessellations. *J. Microsc.* **151**, 187–190.

[17] Miles, R. E. and Mackisack, M. S. (2002). A large class of random tessellations with the classic Poisson polygon distribution. *Forma*, **17**, 1–17.

[18] Møller, J. (1989). Random tessellations in $\mathbb{R}^d$. *Adv. Appl. Prob.* **21**, 37–73.

[19] Muche, L. (1996). The Poisson-Voronoi tessellation II. Edge length distribution functions. *Math. Nachr.* **178**, 271–283.

[20] Muche, L. (1998). The Poisson-Voronoi tessellation III. Miles' formula. *Math. Nachr.* 191, 247–267.

[21] Muche, L. (2005). The Poisson Voronoi tessellation: relationships for edges. *Adv. Appl. Prob.* **37**, 279–296.

[22] Nagel, W. and Weiss, V. (2005). Crack STIT tessellations: characterization of stationary random tessellations stable with respect to iteration. *Adv. Appl. Prob.*, **37**, 859–883.

[23] Nagel, W. and Weiss, V. (2008). Mean values for homogeneous STIT tessellation in 3D. *Image Anal. Stereol.*, **27**, 29–37.

[24] Okabe, A., Boots, B., Sugihara, K. and Chiu, S. N. (2000). *Spatial Tessellations: Concepts and Applications of Voronoi Diagrams.* 2nd. ed., Wiley, Chichester.

[25] Radecke, W. (1980). Some mean-value relations on stationary random mosaics in the space. *Math. Nachr.* **97**, 203–210.

[26] Schneider, R. and Weil, W. (2008). *Stochastic and Integral Geometry.* Springer, Berlin Heidelberg.

[27] Stoyan, D. (1986). On generalized planar random tessellations. *Math. Nachr.* **128**, 215–219.

[28] Stoyan, D., Kendall, W. S. and Mecke, J. (1995). *Stochastic Geometry and its Applications.* 2nd Edition. Wiley, Chichester.

[29] Thäle, C. and Weiss, V. (2010). New mean values for homogeneous spatial tessellations that are stable under iteration. *Image Anal. Stereol.* **29**, 143–157.

[30] Weiss, V. and Zähle, M. (1988). Geometric Measures for Random Curved Mosiacs of $\mathbb{R}^d$. *Math. Nachr.* **138**, 313–326.

[31] Zähle, M. (1988). Random cell complexes and generalised sets. *Ann. Probab.* **16**, 1742–1766.